HHS Public Access

Author manuscript

Kidney Int. Author manuscript; available in PMC 2018 February 01.

Published in final edited form as:

Kidney Int. 2018 February ; 93(2): 375–389. doi:10.1016/j.kint.2017.05.014.

MicroRNA-21 regulates peroxisome proliferator–activated receptor alpha, a molecular mechanism of cardiac pathology in Cardiorenal Syndrome Type 4

Sandra Chuppa[1], **Mingyu Liang**[1,2], **Pengyuan Liu**[1,2], **Yong Liu**[1,2], **Marc C. Casati**[1], **Allen W. Cowley**[1,2], **Leah Patullo**[1], and **Alison J. Kriegel**[1,2]

[1]Department of Physiology, Medical College of Wisconsin, Milwaukee, Wisconsin, USA

[2]Center of Systems Molecular Medicine, Medical College of Wisconsin, Milwaukee, Wisconsin, USA

Abstract

Cardiovascular events are the leading cause of death in patients with chronic kidney disease (CKD), although the pathological mechanisms are poorly understood. Here we longitudinally characterized left ventricle pathology in a 5/6 nephrectomy rat model of CKD and identify novel molecular mediators. Next-generation sequencing of left ventricle mRNA and microRNA (miRNA) was performed at physiologically distinct points in disease progression, identifying alterations in genes in numerous immune, lipid metabolism, and inflammatory pathways, as well as several miRNAs. MiRNA miR-21-5p was increased in our dataset and has been reported to regulate many identified pathways. Suppression of miR-21-5p protected rats with 5/6 nephrectomy from developing left ventricle hypertrophy and improved left ventricle function. Next-generation mRNA sequencing revealed that miR-21-5p suppression altered gene expression in peroxisome proliferator-activated receptor alpha (PPARα) regulated pathways in the left ventricle. PPARα, a miR-21-5p target, is the primary PPAR isoform in the heart, importantly involved in regulating fatty acid metabolism. Therapeutic delivery of low-dose PPARα agonist (clofibrate) to rats with 5/6 nephrectomy improved cardiac function and prevented left ventricle dilation. Thus, comprehensive characterization of left ventricle molecular changes highlights the involvement of numerous signaling pathways not previously explored in CKD models and identified PPARα as a potential therapeutic target for CKD-related cardiac dysfunction.

Keywords

cardiovascular disease; chronic kidney disease; inflammation; renal pathology

Type 4 cardiorenal syndrome (CRS4) is a condition in which chronic kidney disease (CKD) contributes to pathologic cardiac changes, including left ventricular (LV) hypertrophy,

Correspondence: Alison J. Kriegel, Department of Physiology, Medical College of Wisconsin, 8701 Watertown Plank Road, Milwaukee, Wisconsin 53226, USA. akriegel@mcw.edu.

Supplementary References: Supplementary material is linked to the online version of the paper at www.kidney-international.org.

Disclosure: All the authors declared no competing interests.

diastolic dysfunction, reduced cardiac function, and/or an increased risk of adverse cardiovascular events. Cardiovascular events are the leading cause of death among CKD patients, increasing risk by 10 to 20 times, yet little is known about mechanisms that mediate associated cardiac pathology. Common comorbidities in CKD patients, such as hypertension, diabetes, and atherosclerosis, can independently contribute to cardiac risk, making it difficult to elucidate the pathologic mechanisms driving CRS4, the sequence in which other diseases emerge, or their directional causation, in relation to CKD.

The 5/6 nephrectomy (5/6Nx) surgical model of CKD has been shown to induce cardiac remodeling and vascular changes at determined endpoints in several studies, however, longitudinal characterization of cardiac changes has not been reported and alterations in cardiac gene expression accompanying those changes are unknown. Further, several 5/6Nx models induce overt hypertension, making it difficult to identify the underlying mechanisms by which CKD contributes to cardiac pathology and limiting mechanistic understanding of the cause-and-effect relationships. The goal of this study was to use the excision model of 5/6Nx, resulting in only a modest increase in afterload, to comprehensively identify molecular mechanisms that precede or accompany the pathologic changes in (LV structure, composition, and function in response to renal insufficiency. In doing so, we observed a significant increase in miR-21-5p expression in the left ventricle by week 7 post-5/6Nx, a point when pathologic cardiac remodeling has been established. We hypothesized that miR-21-5p is a mediator of LV remodeling and dysfunction through its regulation of peroxisome proliferator-activated receptor-α (PPARα). The downregulation of PPARα has been described in many pathologic processes central to CRS4[13-17]; however, the cardiac implications have never been investigated in an animal model of CKD.

Results

Time-dependent effect of 5/6Nx on kidney and LV remodeling and function

Longitudinal renal and LV changes were characterized by repeated urine and blood collections and echocardiographic analysis (Figure 1a). Body weight was reduced 1 week post-5/6Nx, but rebounded subsequently (Figure 1b). Renal dysfunction was also apparent in 5/6Nx rats, as indicated by polyuria and increased plasma creatinine, urinary/plasma creatinine, protein, and albumin excretion rates (Figure 1c–g). Tubular remodeling and damage scoring (see Supplementary Methods for details) of 5/6Nx remnant kidneys collected during acute studies highlight the large increase in the percentage of proximal tubules exhibiting dilation and/or apical shedding (scores of 4 and 5) at week 7 versus earlier time points (Figure 1h and i).

Longitudinal echocardiographic analysis shows progressive thickening of the LV wall after 5/6Nx, peaking at week 5 and then reversing by week 7 (Figure 2a). Chamber diameter increased as wall thickness decreased (Figure 2b). Ejection fraction increased within the first week, plateaued through week 3 post-5/6Nx, and then decreased in subsequent weeks, returning to baseline by week 7 (Figure 2c). Representative short-axis echocardiography and M-mode images from these time points are shown in Figure 2d.

Sham or 5/6Nx surgery was completed in additional cohorts of rats, followed by echocardiography and terminal hemodynamic and tissue collections 2, 4, and 5 weeks later. These time points were selected to better understand he-modynamic and molecular influences contributing to interesting phenotypic time points identified in the longitudinal study, including the development of hypertrophy at week 3 and maximal hypertrophy at week 5. The average systolic arterial pressure was not increased in 5/6Nx rats until week 5, when an increase of ~15 mm Hg was observed (Figure 2e). Despite diastolic blood pressure (Figure 2f) and heart rate (Figure 2g) remaining unaffected, LV diastolic pressure increased at weeks 5 and 7 (Figure 2h and Supplementary Figure S1). These data suggest that neither preload nor afterload on the left ventricle were significantly altered 2 or 4 weeks after 5/6Nx surgery and that initial LV changes were not driven by volume expansion. Progressive cardiac hypertrophy was evident on echocardiographic analysis (Supplementary Figure S2 and Figure 2a), body weight normalized, and absolute cardiac wet weights (Figure 2i and 2j), and echocardiography calculated LV mass (Figure 2k). Relative wall thickness (LV wall thickness/chamber diameter) calculations suggest a concentric hypertrophic remodeling at weeks 4 and 5 (Figure 2l) that normalizes at week 7 despite an increase in the overall size/mass.

Changes in mRNA expression during disease progression Analysis of mRNA sequencing of pooled LV RNA identified 0, 39, 67, and 220 genes that were significantly differentially expressed 2, 4, 5, and 7 weeks after 5/6Nx, respectively (Supplementary Table S1). The top 10 upregulated and downregulated genes at each time point are listed in Table 1. Ingenuity Pathway Analysis (IPA) was performed using the Ingenuity Knowledge Base, a literature-based compilation of biological interactions and functional ontologies, to identify pathways, diseases, and functions related to measured LV gene expression changes. Several differentially expressed transcripts with functions related to cardiovascular diseases were observed, many at multiple time points (Supplementary Table S3).

Other functions identified by IPA analysis of differentially expressed genes included inflammatory response, immune cell trafficking, and lipid metabolism (Figure 3a-c, respectively). This analysis identified functions that maybe involved with pathology at more than 1 time point in the study, as well as those that were only identified at a specific time point in pathologic progression (Figure 3, bold text).

Pathologic outcomes predicted by early changes in expression pattern

Fibrosis, lipid accumulation, immune cell infiltration, and calcium deposition were evaluated in LV tissue. Although the total percentage of LV fibrosis was not increased by 5/6Nx at any time point (data not shown), evidence of perivascular fibrosis was observed at 7 weeks post-5/6Nx (Figure 4a). The observation of increased lipid in LV tissue only at week 7 (Figure 4b) was consistent with gene expression changes related to lipid metabolism. The 5/6Nx LV tissues also show perivascular the infiltration of CD4 and CD68 immune cells and calcification in both the coronary vascular and myocardial tissue at this time (Figure 4c and d, respectively). The altered genes from our dataset associated with observed pathologies by IPA are summarized in Figure 5.

miR-21-5p suppression with 5/6Nx is cardioprotective

Small RNA deep sequencing was performed on LV RNA at each time point. The top 10 miRNAs that were both detected in all the pools analyzed and altered by an average of at least 1.5-fold in 5/6Nx rats are shown in Figure 6, with a complete list in Supplementary Table S2.

An increase in the abundance of miR-21-5p was identified through small RNA sequencing at 7 weeks post-surgery (Figure 6), a time point where many pathologic changes observed in our study. Increased miR-21-5p has been reported to regulate relevant pathways including immune response[18–21] and lipid metabolism,[22–25] and the abundance of miR-21-5p was high compared with other miRNAs (Supplementary Table S3), suggesting that it may be mediating some cardiac pathology in this model. This finding was validated by realtime quantitative reverse transcription polymerase chain reaction (qRT-PCR) analysis of individual samples from pooled sham and 5/6Nx samples (100 ± 23.8% vs. 329.8 ± 84.2%; N= 6 and 5, respectively). To study the regulatory and functional significance of increased LV miR-21-5p, we delivered a 16-mer anti-miR-21-5p or anti-scrambled (scr) oligonucleotides i.v. to sham or 5/6Nx rats (Figure 7a). This treatment protocol effectively suppressed miR-21-5p through the end of the 7-week study (Figure 7b) without affecting the abundance of miR-21-3p (Supplementary Figure S3), suggesting specificity for the mature miRNA Anti-miR-21-5p also had a similar suppressive effect in the kidney, where we also observed an increase in miR-21-5p 7 weeks post-5/6Nx (Supplementary Figure S3).

Because miR-21-5p abundance was also increased in the kidney of 5/6Nx rats, we evaluated several measures of renal function in response to miR-21-5p suppression. Anti–miR-21-5p reduced body weight compared with anti–scr-treated controls (Figure 7c), but had little impact on 24-hour urine volumes or plasma creatinine (Figure 7d and e). Further, urinary protein and albumin excretion rates (Figure 7f and g) and renal morphology/fibrosis (Figure 7m and n) were not altered by anti–miR-21-5p treatment. Cardiac remodeling was also evaluated longitudinally. At week 7, anti–miR-21-5p treatment maintained LV wall thickness (Figure 7h) and chamber diameter (Figure 7i) while increasing the ejection fraction (Figure 7j). Anti–mR-21 delivery in sham rats had no effect on any of these parameters. Interestingly, anti–miR-21-5p increased the systolic/diastolic wall thickness ratio in 5/6Nx rats at weeks 5 and 7, suggesting enhanced systolic contraction (Figure 7k). Blood pressure (Figure 7l) was not reduced by anti–miR-21-5p treatment. Together these findings indicate that changes in cardiac phenotypes with anti–miR-21-5p were not driven by a reduction in renal injury.

miR-21-5p effect on fibrosis and hypertrophy

We investigated the effect of miR-21-5p on LV fibrosis and hypertrophy in our 5/6Nx model. These pathologic processes were previously reported to be regulated by miR-21-5p.

We find that the very small amount of perivascular fibrosis that develops with 5/6Nx was not reduced with anti–miR-21-5p treatment (Figure 8a). Cross-sectional LV cardiomyocyte area, as a measure of cardiomyocyte hypertrophy, was reduced with anti–miR-21-5p treatment, although myocyte area remained higher than sham-operated controls (Figure 8b). To better

understand the role of miR-21-5p in hypertrophy, we studied the effect of miR-21-5p on the H9C2 cell area in response to insulin-like growth factor-1 treatment. The H9C2 cell line has been shown have a hypertrophic response, similar to primary neonatal cardiomyocytes.[26] Transfection of cells with anti–miR-21-5p completely prevented an increase in the H9C2 area in response to a subsequent 24-hour insulin-like growth factor-1 (50 ng/ml) treatment (Figure 8c).

miR-21-5p targets LV PPARα

Next-generation mRNA sequencing was performed on anti– scr or anti–miR-21-5p treated LV samples to identify potential miR-21-5p targets (Supplementary Table S4). We found no overlap between Targetscan-predicted miR-21-5p targets and the list of transcripts that were upregulated >1.5-fold and related to cardiac function, prompting us to use IPA analysis to identify translationally repressed targets. Translational repression by an miRNA can reduce protein abundance without reducing mRNA abundance. Pathways involved with inflammation, atherosclerosis, the immune system, and metabolism were enriched with mRNAs altered by > 1.25-fold with anti-miR-21-5p. We identified PPARα as candidate that is both a translationally repressed target of miR-21-5p and has a known regulator of pathways listed previously.[25,27]

Protein expression of LV PPARα was significantly reduced with 5/6Nx only at week 7, when miR-21-5p was increased in our LV tissue and not at earlier time points (Figure 9a). Suppression of miR-21-5p with locked nucleic acid-modified anti-miR-21-5p had no effect in sham animals (Figure 8b), but increased PPARα levels in 5/6Nx rats (Figure 9c). The abundance of PPARα mRNA transcript was unaffected by anti-miR-21-5p in 5/6Nx rats when evaluated by qRT-PCR analysis (100 ± 15.4%, anti-scr vs. 86.8 ± 4.5% anti-miR-21-5p), consistent the mRNA sequencing results. Transfection of neonatal rat cardiomyocytes with pre-miR-21-5p to increased miR-21-5p abundance 113.5 ± 68.2-fold (vs. pre-scr), resulting in a significant reduction in PPARα (Figure 9d). These data are consistent with miR-21-5p regulation of PPARα. Finally, although miR-21-5p has been previously shown to target human PPARα through translational repression,[25,27] and binding sequences are conserved between human, mouse, and rat (http://www.targetscan.org), we confirmed this regulatory interaction by performing 3′-un-translated region (3′-UTR). Both full and partial rat 3′-UTR sequences were regulated by anti-miR-21 in this analysis (6.2 ± 0.2% and 7.1 ± 0.2, respectively; percentage of change with anti-miR-21-5p vs. pre-scr treatment; $P < 0.05$, Student t test; $N = 7$-9 per group).

Therapeutic restoration of PPARα signaling improves LV function

Having identified PPARα as a direct miR-21-5p target in this model, we tested therapeutic PPARα activation by delivering a low therapeutic dose (25 mg/kg) of the PPARα agonist clofibrate via daily i.p. injections starting 5 weeks post-surgery, a time point before the increase in miR-21-5p observed at week 7, and continuing through the end of the 10-week study. This dose is approximately 1/10th of the dose commonly given to rats ~ 3 because toxicity was observed at a higher concentration (data not shown), most likely due to impaired renal clearance. [1,3] Clofibrate treatment did not reduce plasma creatinine levels in the 5/6Nx rats (Figure 9e), but it did significantly reduce urinary protein and albumin

(Figure 9f and g, respectively). Clofibrate treatment in 5/6Nx animals prevented the decrease in ejection fraction observed in controls (Figure 9h). Similarly, treated 5/6Nx rats developed less LV dilation (Figure 9i) and had a significantly increased systolic wall thickness (Figure 9j), similar to the rats treated with anti–miR-21-5p (Figure 7). The systolic and diastolic blood pressures in 5/6Nx rats were unaffected by clofibrate treatment, suggesting that reduced afterload was not responsible for the observed cardiac benefit.

Discussion

Cardiac remodeling and dysfunction in CRS4 have been largely attributed to dramatic changes in volume status or blood pressure.[33–35] However, this does not appear to be a prerequisite for all changes in gene expression and function based on our observations. Animals subjected to 5/6Nx are polyuric, and body weight measurements tend to be lower compared when controls, suggesting that they are not volume expanded. The modest increases in anesthetized blood pressure observed at weeks 5 and 7 were not accompanied by interstitial fibrosis, the classic sign of pressure-overloading pathology. Although anesthesia may have an impact on blood pressure measurements, the surgical excision 5/6Nx model used in this study has been shown to induce CKD-related pathology without increasing blood pressure in conscious animals.[36]

Cumulatively, our observations indicate that the changes in LV function and gene expression, many of which occurred before weeks 5 and 7, were not driven simply by hemodynamic changes. Rather, complex alterations in inflammation, immune responses, lipid metabolism, and other pathologic processes were initially observed well before those points, as summarized in Figure 6. Our data suggest that CKD-related cardiac pathology develops, at least in part, as a consequence of several nonhemodynamic processes that were initiated as an early response to reduced renal function (Figure 6). This is consistent with findings by Kennedy *et al.*[9] showing that ischemic 5/6Nx produced greater cardiac hypertrophy (by mass) than aortic constriction, despite similarly elevated mean arterial pressures. Further, a recent study by Park *et al.*[37] showed that cardiac remodeling occurred at all stages of CKD, but became more prevalent with advanced CKD, suggesting that the development of CRS4 is progressive.

Evidence of renal-initiated cardiac innate and adaptive immune responses

The gene expression changes most frequently observed in our analysis were those related to innate and adaptive immune responses. The involvement of the immune system in crosstalk between the kidney and cardiovascular system is widely recognized in CKD. An inflammatory state has been described in hemodialysis patients as well patients with early stages of CKD[38] and in the 5/6Nx model.[39] Our study provides the first comprehensive data showing that primary renal insufficiency can drive broad changes in the LV immune-related gene expression weeks before immune cells are observed in the tissue. The molecular signals driving these changes were not evaluated in this study, although several circulating factors, such as Klotho,[40] fibroblast growth factor 23,[40–42] and uremic toxins,[43] have been implicated in the development of CRS4.

miRNA regulation of LV PPARα in the 5/6Nx model

miRNA exerts posttranscriptional regulation primarily through interaction with the 3′ -UTR of protein-coding mRNAs. Mechanisms of miRNA regulation vary, but they generally reduce the expression of a targeted mRNA by suppressing translation, leaving the mRNA transcript unchanged, or by promoting mRNA degradation. RNA sequencing can detect changes in miRNA-targeted mRNAs that are regulated via transcript degradation; however, this is not possible for miRNA targets that are translationally repressed. Despite this limitation, the RNA sequencing will detect changes in mRNAs within pathways related to a translationally repressed target, allowing researchers to narrow in on a subset of predicted targets. Our pathway-focused analysis of transcript abundance changes within mRNA sequencing data allowed us to identify miR-21-5p–mediated translational repression of PPARa as an important regulatory mechanism in the 5/6Nx model of CKD. miR-21-5p has a role in acute and chronic pathology in several organs. Short term cardiac upregulation of miR-21-5p is protective in ischemia/reperfusion injury, while chronic upregulation has been associated with pathologic changes.[24,44] miR-21-5p suppression has also been reported to be renoprotective in models of acute renal injury/fibrosis[24] and Alport nephropathy[45]; however, we did not observe improved renal function or reduced renal fibrosis in this study (Figure 7e,f,m,n). This is likely due to substantial differences in disease models, the pathologic stimuli involved, and the rates of pathology progression between studies.

In the left ventricle, upregulation of miR-21-5p has been observed in rodent models of pressure overloading (PO) and volume overloading.[46,47] The significance of miR-21-5p in PO hypertrophy has remained uncertain due to conflicting studies using different molecular approaches to suppress miR-21-5p in vivo.[48,49] Here, we use the treatment protocol and locked nucleic acid chemistry similar to those used by Patrick *et al.*[48] in a study that found that miR-21-5p suppression had no effect on PO pathology. Our findings indicate a cardioprotective effect in 5/6Nx, but cannot resolve the inconsistent findings previously reported in PO models. The hemodynamic and circulating factors in our CKD model are distinctly different from the conditions of cardiac stress and PO used in those studies; however, we did observe 2 interesting findings. First, chronic knockdown of miR-21-5p prevented hypertrophic remodeling of the LV wall at week 5 post-5/6Nx (Figure 7), and subsequently the average cardiomyocyte cross-sectional area measured at 7 weeks was lower than that of anti–scr-treated rats (Figure 8a). Second, anti–miR-21-5p knockdown prevented subsequent insulinlike growth factor-1–induced increases in a cultured H9C2 cell area, a surrogate for hypertrophy in vitro (Figure 8c). This suggests that physiologic levels of miR-21-5p may be required to facilitate subsequent hypertrophic growth under certain pathologic conditions.

The upregulation of miR-21-5p has been associated with CKD[50,51] as well as atherosclerotic development.[52,53] Suppression of miR-21-5p did not improve the numerous measured indices of renal function or reduce blood pressure, suggesting that cardiac benefits of anti–miR-21-5p were not the result of indirect improvements in renal function or reduced afterload. PPARα is a confirmed target of miR-21-5p, and this targeting can contribute to liver steatosis as renal fibrosis in unilateral ureteral obstruction and unilateral ischemia/reperfusion models of renal fibrosis.[24,54] The association of reduced cardiac PPARα

expression with inflammation, atherosclerosis, and pathologic shifts from fatty acid oxidation to glycolysis is well established.[13–16,55]

Clofibrate is a synthetic PPARα agonist that induces heterodimerization of the nuclear receptor with retinoid-X receptors. This heterodimer binds peroxisome proliferator–response elements within the genome to regulate transcription of numerous genes related to fatty acid uptake and oxidation, inflammation, and vascular function. Comprehensive proteomic analysis of changes in protein expression in LV tissue induced by clofibrate treatment show alterations in numerous proteins involved in these processes.[56] We observed that clofibrate treatment (Figure 9 e–k), which was not initiated until >5 weeks after 5/6Nx surgery, increased systolic wall thickness and significantly reduced LV dilation measured 10 weeks after surgery. These changes ultimately contributed to an improved ejection fraction. A previous study on cardiac ischemia showed that clofibrate treatment similarly improved cardiac function after myocardial infarction.[57] Treatment of 5/6Nx rats had no impact on plasma creatinine levels, however urinary protein and albumin excretion rates were significantly reduced, suggesting an improvement in renal function that was not observed with miR-21-5p suppression. The mechanisms responsible for this improvement in renal function on cardiac function require further investigation.

In summary, this study provides the first comprehensive analysis of cardiac mRNA and miRNA expression changes throughout the development of cardiac pathology in the 5/6Nx model of CRS4. Understanding how these changes contribute to cardiac pathology will be of great importance when treating patients with CKD. We have identified miR-21-5p–mediated targeting of PPARα using this approach and shown a therapeutic benefit of administering a PPARα agonist during cardiac remodeling in a rat model of CKD. These data suggest that therapeutic restoration of PPARα signaling, via low-dose fibrate therapy, may be beneficial in CKD patients exhibiting hypertrophic cardiac remodeling. Further research on the molecular changes identified in our analysis may elucidate additional therapeutic targets that reduce cardiac pathology induced by the progressive development of CKD.

Methods

Animal model

Animal protocols were approved by the MCW Institutional Animal Care and Use Committee. Male Sprague Dawley rats ($N = 110$) (Harlan Sprague Dawley, Madison, WI) were fed 0.4% NaCl diet (AIN-76A Purified Rodent Diet, Dyets, Inc., Bethlehem, PA) and provided water ad libitum. At 10 weeks of age, rats were anesthetized by i.m. injection of a ketamine (50 mg/kg)/xylazine (8 mg/kg)/acepromazine (5 mg/kg) mixture and subjected to sham or 5/6Nx surgery using a surgical excision model, as previously described.[36] Briefly, the right kidney was removed and two-thirds (upper and lower poles) of the left kidney were removed by scalpel excision. Gelfoam coagulant was applied to the cut surfaces.

Longitudinal studies

Phenotypic measurements, including 24-hour urine collections in metabolic cages, 2-dimensional echocardiography (VIVID 7, GE Healthcare, Chicago, IL), and blood

collection, were performed as in Figure 1a or as indicated. Echocardiography and blood collection were performed with rats under anesthesia, as described previously. Plasma and urine creatinine was measured using the QuantiChrome Creatinine Assay Kit (BioAssay Systems LLC, Hayward, CA), based on the Jaffe method. Urine collections and subsequent protein and creatinine excretion measurements were performed as previously described.[58]

Acute studies for LV mRNA and miRNA analysis

Separate groups of animals were studied at weeks 2, 4, 5, and 7 post-sham or 5/6Nx surgery to make invasive cardiac measurements and for LV tissue collection for gene/miRNA expression analysis. After echocardiography at these time points, anesthetized blood pressure and end-diastolic LV pressures were averaged from 30 seconds of stable recording by a 9F catheter (Millar, Inc., Houston, TX) inserted retrograde through the carotid artery. Animals were subsequently killed, and tissue was collected.

Anti–miR-21-5p delivery

Locked nucleic acid–modified anti–miR-21-5p or anti-scr (Exiqon, Vedbaek, Denmark), in saline, were delivered i.v. through a jugular catheter using a treatment protocol similar to that reported by Patrick *et al.*[48] (1 mg/kg per day in 3 daily injections), as shown in Figure 7a. Longitudinal studies were repeated as described previously.

Hypertrophy analysis

Wheat germ agglutinin staining was performed on LV tissue sections for imaging.[59] H9C2 cardiac myoblast cells (ATCC) were transfected with anti-scr or anti–miR-21-5p (40 nM, Exiqon, Vedbaek, Denmark), as previously described.[60] After 48 hours, cells were treated with insulin-like growth factor-1 (50 ng/ml; StemRD, Burlingame, CA) or saline vehicle for an additional 24 hours ($N = 3$ per group). Cells were fixed and imaged. At least 10 images were captured and quantified per tissue/replicate. Metamorph software was used for quantification.

Clofibrate treatment

Clofibrate (25 mg/kg per day) or saline was delivered via daily i.p. injection beginning on day 39 and continuing until the study ended at 10 weeks post-surgery.

Tissue collection and histology

The heart and remnant kidney (or left kidney, sham) were collected at the indicated time points, weighed, and sectioned for histology, RNA, and protein analysis, as previously descibed.[61] See Supplementary Methods for tubular scoring. Perivascular fibrosis was quantified, and immunohistochemistry (antibodies from Santa Cruz Biotechnology, Dallas, TX) was performed, as previously described. Oil Red O staining was used to visualize LV lipid content. Calcium deposition was evaluated by von Kossa staining with an eosin counterstain.[63]

Statistical analysis of physiological and histologic data

One- or 2-way repeated-measures analysis of variance was used in the analysis of longitudinally collected data. The Student *t* test was used for single comparisons, and multiple comparisons were analyzed by 1-way analysis of variance at a single time point. Data are given as mean ± SEM, with a threshold for significant differences set at $P < 0.05$.

Next-generation sequencing, mRNA and miRNA analysis

Total LV RNA was extracted, as previously described and quantified by NanoDrop (Thermo Fisher Scientific, Waltham, MA). RNA from 2 to 3 animals was pooled in equal amounts to generate 2 pools of RNA from sham and 5/6Nx groups at each time point studied (i.e., 2, 4, 5, and 7 weeks post-surgery [Supplementary Table S1]). Details of mRNA sequencing are provided in Supplementary Methods and Supplementary Table S5. Small RNA deep sequencing was performed as previously described,[64] and Targetscan (http://www.targetscan. org) was used to identify miRNA targets.[61] Details of RNA-seq and 3′-UTR analysis are provided in Supplementary Methods and Supplementary Table S6. Taqman miRNA assays (ThermoFisher, Waltham, MA) were used measure miR-21-5p and -3p abundance, as previously described.[61] PPARα transcript was measured by qRT-PCR, as previously described,[61,65] using ribosomal 18s transcript as a normalization control) (forward primer 5′-TCCAGCCCCTCCT-CAGTCA-3′; reverse primer 5′-AGCCCTTGCAGCCTTCACA-3′).

Pathway analysis of differentially expressed transcripts

A list of differentially expressed miRNAs and log fold change were uploaded to IPA for Downstream Effects Analysis. Diseases and functions identified as statistically significant IPA were included in the analysis.

Western blot

Neonatal rat cardiomyocytes were transfected with 20 nM pre-miR-21-5p or scr control ($N = 3$ per group) (ThermoFisher) as previously described[60] and collected 48 hours later. Tissue and cell material were processed for Western blot analysis as previously described, with quantification of Coomassie staining used as to normalize protein loaded.[61]

Supplementary Material

Refer to Web version on PubMed Central for supplementary material.

Acknowledgments

Support received from the American Heart Association 13SDG17100095 (AJK), National Institutes of Health 8UL1TR000055 (AJK), and R01HL128332 (AJK) and R01 HL121233 (ML), P01 GM066730-8167 (ML), and P01 HL082798-6186 (ML).The authors thank Jessica Olson for providing neonatal cardiomyocytes for these studies.

References

1. Foley RN, Parfrey PS, Sarnak MJ. Clinical epidemiology of cardiovascular disease in chronic renal disease. Am J Kidney Dis. 1998; 32:S112–S119. [PubMed: 9820470]

2. Owan TE, Hodge DO, Herges, et al. Secular trends in renal dysfunction and outcomes in hospitalized heart failure patients. J Card Fail. 2006; 12:257–262. [PubMed: 16679257]

3. Krumholz HM, Chen YT, Vaccarino V, et al. Correlates and impact on outcomes of worsening renal function in patients > or ¼65 years of age with heart failure. Am J Cardiol. 2000; 85:1110–1113. [PubMed: 10781761]

4. Nohria A, Hasselblad V, Stebbins A, et al. Cardiorenal interactions: insights from the ESCAPE trial. J Am Coll Cardiol. 2008; 51:1268–1274. [PubMed: 18371557]

5. Butler J, Forman DE, Abraham WT, et al. Relationship between heart failure treatment and development of worsening renal function among hospitalized patients. Am Heart J. 2004; 147:331–338. [PubMed: 14760333]

6. Forman DE, Butler J, Wang Y, et al. Incidence, predictors at admission, and impact of worsening renal function among patients hospitalized with heart failure. J Am Coll Cardiol. 2004; 43:61–67. [PubMed: 14715185]

7. Tornig J, Amann K, Ritz E, et al. Arteriolar wall thickening, capillary rarefaction and interstitial fibrosis in the heart of rats with renal failure: the effects of ramipril, nifedipine and moxonidine. J Am Soc Nephrol. 1996; 7:667–675. [PubMed: 8738800]

8. Sviglerova J, Kuncova J, Nalos L, et al. Cardiovascular parameters in rat model of chronic renal failure induced by subtotal nephrectomy. Physiol Res Acad Sci Bohemoslov. 2010; 59(Suppl 1):S81–S88.

9. Kennedy D, Omran E, Periyasamy SM, et al. Effect of chronic renal failure on cardiac contractile function, calcium cycling, and gene expression of proteins important for calcium homeostasis in the rat. J Am Soc Nephrol. 2003; 14:90–97. [PubMed: 12506141]

10. Gut N, Piecha G, Aldebssi F, et al. Erythropoietin combined with ACE inhibitor prevents heart remodeling in 5/6 nephrectomized rats independently of blood pressure and kidney function. Am J Nephrol. 2013; 38:124–135. [PubMed: 23920063]

11. Baraka A, El Ghotny S. Cardioprotective effect of renalase in 5/6 nephrectomized rats. J Cardiovasc Pharmacol Ther. 2012; 17:412–416. [PubMed: 22626958]

12. Drummond CA, Buddny G, Haller ST, et al. Gender differences in the development of uremic cardiomyopathy following partial nephrectomy: role of progesterone. J Hypertens (Los Angel). 2013:2.

13. Karbowska J, Kochan Z, Smolenski RT. Peroxisome proliferator-activated receptor alpha is downregulated in the failing human heart. Cell Mol Biol Lett. 2003; 8:49–53. [PubMed: 12655356]

14. Delerive P, De Bosscher K, Besnard S, et al. Peroxisome proliferator-activated receptor alpha negatively regulates the vascular inflammatory gene response by negative cross-talk with transcription factors NF-kappaB and AP-1. J Biol Chem. 1999; 274:32048–32054. [PubMed: 10542237]

15. Youssef J, Badr M. Role of peroxisome proliferator-activated receptors in inflammation control. J Biomed Biotechnol. 2004; 2004:156–166. [PubMed: 15292582]

16. Guellich A, Damy T, Lecarpentier Y, et al. Role of oxidative stress in cardiac dysfunction of PPARalpha-/- mice. Am J Physiol Heart Circ Physiol. 2007; 293:H93–H102. [PubMed: 17369471]

17. Cao H, Wen G, Li H, et al. Role of peroxisome proliferator-activated receptor alpha in atherosclerosis. Mol Med Rep. 2014; 9:1755–1760. [PubMed: 24604149]

18. Sheedy FJ, Palsson-McDermott E, Hennessy EJ, et al. Negative regulation of TLR4 via targeting of the proinflammatory tumor suppressor PDCD4 by the microRNA miR-21. Nat Immunol. 2010; 11:141–147. [PubMed: 19946272]

19. Das A, Ganesh K, Khanna S, et al. Engulfment of apoptotic cells by macrophages: a role of microRNA-21 in the resolution of wound inflammation. J Immunol. 2014; 192:1120–1129. [PubMed: 24391209]

20. Lu TX, Munitz A, Rothenberg ME. MicroRNA-21 is up-regulated in allergic airway inflammation and regulates IL-12p35 expression. J Immunol. 2009; 182:4994–5002. [PubMed: 19342679]

21. Lu TX, Hartner J, Lim EJ, et al. MicroRNA-21 limits in vivo immune response-mediated activation of the IL-12/IFN-gamma pathway, Th1 polarization, and the severity of delayed-type hypersensitivity. J Immunol. 2011; 187:3362–3373. [PubMed: 21849676]

22. Feng J, Li A, Deng J, et al. miR-21 attenuates lipopolysaccharide-induced lipid accumulation and inflammatory response: potential role in cerebrovascular disease. Lipids Health Dis. 2014; 13:27. [PubMed: 24502419]
23. Calo N, Ramadori P, Sobolewski C, et al. Stress-activated miR-21/miR-21* in hepatocytes promotes lipid and glucose metabolic disorders associated with high-fat diet consumption. Gut. 2016; 65:1871–1881. [PubMed: 27222533]
24. Chau BN, Xin C, Hartner J, et al. MicroRNA-21 promotes fibrosis of the kidney by silencing metabolic pathways. Sci Transl Med. 2012; 4:121r. a18.
25. Kida K, Nakajima M, Mohri T, et al. PPARalpha is regulated by miR-21 and miR-27b in human liver. Pharm Res. 2011; 28:2467–2476. [PubMed: 21562928]
26. Watkins SJ, Borthwick GM, Arthur HM. The H9C2 cell line and primary neonatal cardiomyocyte cells show similar hypertrophic responses in vitro. In Vitro Cell Dev Biol Anim. 2011; 47:125–131. [PubMed: 21082279]
27. Zhou J, Wang KC, Wu W, et al. MicroRNA-21 targets peroxisome proliferators-activated receptor-alpha in an autoregulatory loop to modulate flow-induced endothelial inflammation. Proc Natl Acad Sci. U S A. 2011; 108:10355–10360.
28. Leonard JF, Courcol M, Mariet C, et al. Proteomic characterization of the effects of clofibrate on protein expression in rat liver. Proteomics. 2006; 6:1915–1933. [PubMed: 16470657]
29. Newaz MA, Ranganna K, Oyekan AO. Relationship between PPARalpha activation and NO on proximal tubular Naþ transport in the rat. BMC Pharmacol. 2004; 4:1. [PubMed: 15018640]
30. Garnier A, Poizat C, Keriel C, et al. Modulation of fatty acid-binding protein content of adult rat heart in response to chronic changes in plasma lipid levels. Mol Cell Biochem. 1993; 123:107–112. [PubMed: 8232251]
31. Goldberg AP, Sherrard DJ, Haas LB, Brunzell JD. Control of clofibrate toxicity in uremic hypertriglyceridemia. Clin Pharmacol Ther. 1977; 21:317–325. [PubMed: 837651]
32. Sherrard DJ, Goldberg AB, Haas LB, Brunzell JD, et al. Chronic clofibrate therapy in maintenance hemodialysis patients. Nephron. 1980; 25:219–221. [PubMed: 7383233]
33. Levey AS, Coresh J, Balk E, et al. National Kidney F. National Kidney Foundation practice guidelines for chronic kidney disease: evaluation, classification, and stratification. Ann Intern Med. 2003; 139:137–147. [PubMed: 12859163]
34. Ronco C, Haapio M, House AA, et al. Cardiorenal syndrome. J Am Coll Cardiol. 2008; 52:1527–1539. [PubMed: 19007588]
35. Ronco C, Maisel A. Volume overload and cardiorenal syndromes. Congest Heart Failure. 2010; 16(Suppl 1) Si–Siv; quiz Svi.
36. Griffin KA, Picken M, Bidani AK. Method of renal mass reduction is a critical modulator of subsequent hypertension and glomerular injury. J Am Soc Nephrol. 1994; 4:2023–2031. [PubMed: 7919155]
37. Park M, Hsu CY, Li Y, et al. Chronic Renal Insufficiency Cohort Study G. Associations between kidney function and subclinical cardiac abnormalities in CKD. J Am Soc Nephrol. 2012; 23:1725–1734. [PubMed: 22935481]
38. Colombo PC, Ganda A, Lin J, et al. Inflammatory activation: cardiac, renal, and cardio-renal interactions in patients with the cardiorenal syndrome. Heart Fail Rev. 2012; 17:177–190. [PubMed: 21688186]
39. Mu W, Ouyang X, Agarwal A, et al. IL-10 suppresses chemokines, inflammation, and fibrosis in a model of chronic renal disease. J Am Soc Nephrol. 2005; 16:3651–3660. [PubMed: 16251240]
40. Xie J, Yoon J, An SW, et al. Soluble Klotho protects against uremic cardiomyopathy independently of fibroblast growth factor 23 and phosphate. J Am Soc Nephrol. 2015; 26:1150–1160. [PubMed: 25475745]
41. Gutierrez OM, Januzzi JL, Isakova T, et al. Fibroblast growth factor 23 and left ventricular hypertrophy in chronic kidney disease. Circulation. 2009; 119:2545–2552. [PubMed: 19414634]
42. Stevens KK, McQuarrie EP, Sands W, et al. Fibroblast growth factor 23 predicts left ventricular mass and induces cell adhesion molecule formation. Int J Nephrol. 2011; 2011:297070. [PubMed: 21860794]

43. Lekawanvijit S, Kompa AR, Wang BH, et al. Cardiorenal syndrome: the emerging role of protein-bound uremic toxins. Circ Res. 2012; 111:1470–1483. [PubMed: 23139286]
44. Xu X, Kriegel AJ, Jiao X, et al. miR-21 in Ischemia/reperfusion injury: a double-edged sword? Physiol Genomics. 2014; 46:789–797. [PubMed: 25159851]
45. Gomez IG, MacKenna DA, Johnson BG, et al. Anti-microRNA-21 oligonucleotides prevent Alport nephropathy progression by stimulating metabolic pathways. J Clin Invest. 2015; 125:141–156. [PubMed: 25415439]
46. van Rooij E, Sutherland LB, Liu N, et al. A signature pattern of stress-responsive microRNAs that can evoke cardiac hypertrophy and heart failure. Proc Natl Acad Sci U S A. 2006; 103:18255–18260. [PubMed: 17108080]
47. Toischer K, Rokita AG, Unsold B, et al. Differential cardiac remodeling in preload versus afterload. Circulation. 2010; 122:993–1003. [PubMed: 20733099]
48. Patrick DM, Montgomery RL, Qi X, et al. Stress-dependent cardiac remodeling occurs in the absence of microRNA-21 in mice. J Clin Invest. 2010; 120:3912–3916. [PubMed: 20978354]
49. Thum T, Gross C, Fiedler J, et al. MicroRNA-21 contributes to myocardial disease by stimulating MAP kinase signalling in fibroblasts. Nature. 2008; 456:980–984. [PubMed: 19043405]
50. Glowacki F, Savary G, Gnemmi V, et al. Increased circulating miR-21 levels are associated with kidney fibrosis. PloS One. 2013; 8:e58014. [PubMed: 23469132]
51. Zawada AM, Rogacev KS, Muller S, et al. Massive analysis of cDNA Ends (MACE) and miRNA expression profiling identifies proatherogenic pathways in chronic kidney disease. Epigenetics. 2014; 9:161–172. [PubMed: 24184689]
52. Ji R, Cheng Y, Yue J, et al. MicroRNA expression signature and antisense-mediated depletion reveal an essential role of MicroRNA in vascular neointimal lesion formation. Circ Res. 2007; 100:1579–1588. [PubMed: 17478730]
53. Raitoharju E, Lyytikainen LP, Levula M, et al. miR-21, miR-210, miR-34a, and miR-146a/b are up-regulated in human atherosclerotic plaques in the Tampere Vascular Study. Atherosclerosis. 2011; 219:211–217. [PubMed: 21820659]
54. Loyer X, Paradis V, Henique C, et al. Liver microRNA-21 is overexpressed in non-alcoholic steatohepatitis and contributes to the disease in experimental models by inhibiting PPARalpha expression. Gut. 2015
55. Djouadi F, Brandt JM, Weinheimer CJ, et al. The role of the peroxisome proliferator-activated receptor alpha (PPAR alpha) in the control of cardiac lipid metabolism. Prostaglandins Leukot Essent Fatty Acids. 1999; 60:339–343. [PubMed: 10471118]
56. Miyazaki M, Nakagawa I, Koga S, et al. Proteomics analysis of cardiac muscle from rats with peroxisomal proliferator-activated receptor alpha (PPARalpha) stimulation. J Toxicol Sci. 2010; 35:131–135. [PubMed: 20118634]
57. Tian Q, Grzemski FA, Panagiotopoulos S, Ahokas JT. Peroxisome proliferator-activated receptor alpha agonist, clofibrate, has profound influence on myocardial fatty acid composition. Chem Biol Interact. 2006; 160:241–251. [PubMed: 16540100]
58. Geurts AM, Mattson DL, Liu P, et al. Maternal diet during gestation and lactation modifies the severity of salt-induced hypertension and renal injury in Dahl salt-sensitive rats. Hypertension. 2015; 65:447–455. [PubMed: 25452472]
59. Ucar A, Gupta SK, Fiedler J, et al. The miRNA-212/132 family regulates both cardiac hypertrophy and cardiomyocyte autophagy. Nat Commun. 2012; 3:1078. [PubMed: 23011132]
60. Olson JM, Yan Y, Bai X, et al. Up-regulation of microRNA-21 mediates isoflurane-induced protection of cardiomyocytes. Anesthesiology. 2015; 122:795–805. [PubMed: 25536091]
61. Kriegel AJ, Liu Y, Cohen B, et al. MiR-382 targeting of kallikrein 5 contributes to renal inner medullary interstitial fibrosis. Physiol Genomics. 2012; 44:259–267. [PubMed: 22202692]
62. Lillie R, Ashburn L. Supersaturated solutions of fat stains in dilute isopropanol for demonstration of acute fatty degeneration not shown by Herxheimer's technique. Arch Pathol. 1943:432–440.
63. Sheehan, DC. Theory and Practice of Histotechnology. 2nd. Battelle Press, Ohil; 1980. p. 226-227.
64. Kriegel AJ, Liu Y, Liu P, et al. Characteristics of microRNAs enriched in specific cell types and primary tissue types in solid organs. Physiol Genomics. 2013; 45:1144–1156. [PubMed: 24085797]

65. Kriegel AJ, Baker MA, Liu Y, et al. Endogenous microRNAs in human microvascular endothelial cells regulate mRNAs encoded by hypertension-related genes. Hypertension. 2015; 66:793–799. [PubMed: 26283043]

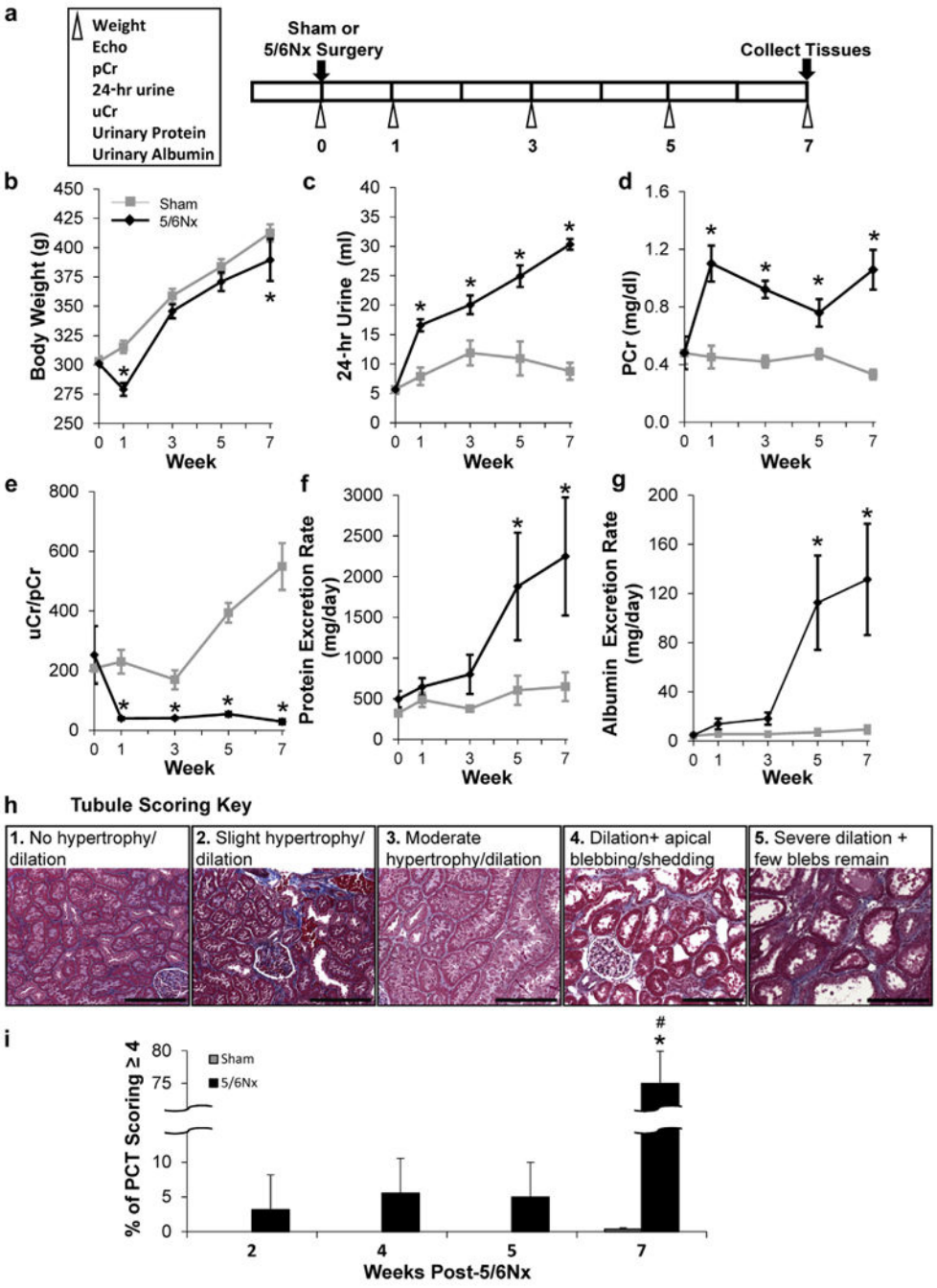

Figure 1. 5/6Nx induces progressive renal pathology

Phenotyping protocol used (**a**). (**b**) Repeated phenotypic measurements of body weight and indices of impaired renal function with 5/6Nx including increased 24-hour urine volume (c), increased plasma creatinine levels (d), a reduced urinary to plasma creatinine ratio (uCr/pCr) (**e**), progressively increasing protein (**f**), and albumin excretion rates (**g**). $N = 5–6$ per group; *P< 0.05 versus sham controls; 2-way repeated-measures analysis of variance. Renal pathology was evaluated in animals used for LV gene expression analysis at weeks 2, 4, 5, and 7 post-5/6Nx. Proximal tubular damage including pronounced dilation, apical blebbing,

and loss of brush border (damage score of 4–5) was extensive 7 weeks after 5/6Nx surgery and not at early time points studied. Tubular scoring key (**h**). Weeks post-5/6NX (i). $N = 5–6$ per group; *P < 0.05 versus sham controls; $^{\#}P < 0.05$ versus 5/6Nx at 2, 4, and 5 weeks; 2-way analysis of variance. 5/6Nx, 5/6 nephrectomy; Echo, echocardiogram; PCT, proximal convoluted tubules. Bar = 200 μm. To optimize viewing of this image, please see the online version of this article at www.kidney-international.org.

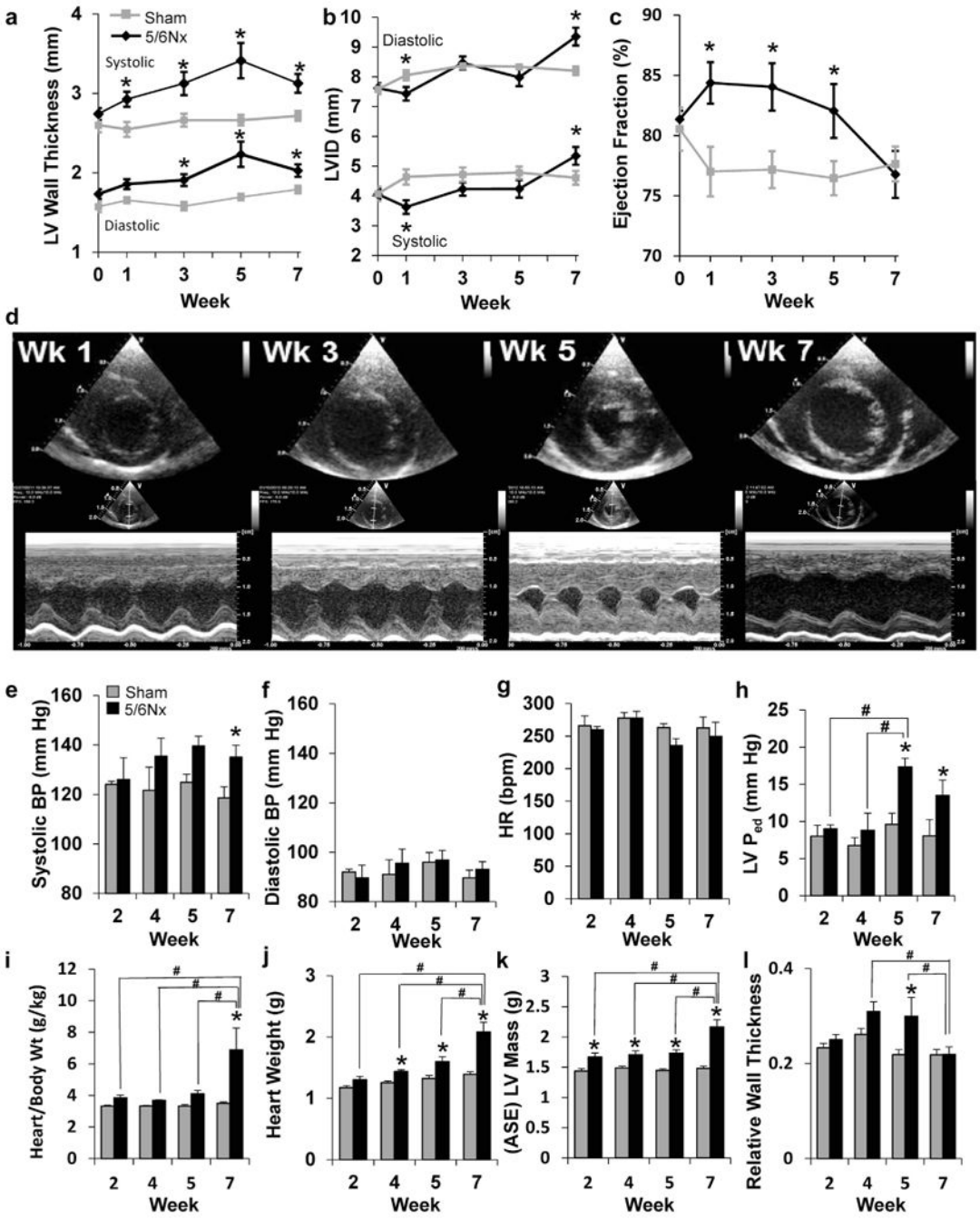

Figure 2. Indices of left ventricular (LV) remodeling and function

(a) Measurements of wall thickness, (**b**) LV inner diameter (LVID), and (**c**) percentage of ejection fraction were made from M-mode echocardiography images before surgery and at weeks 1, 3, 5, and 7 post-surgery. $N = 12$ per group; $^{*}P < 0.05$ versus sham controls; 2-way repeated-measures analysis of variance. (d) Representative echocardiograms of end-diastolic dimension show dramatic changes inboth wall thickness and chamber size inresponse to 5/6 nephrectomy (5/6Nx) (upper, short-axis view; lower, M-mode view). Hemodynamic influences on the left ventricle were measured in animals before tissue collection for gene

expression analysis at weeks 2, 4, 5, and 7 post-5/6Nx. (**e**) Systolic blood pressure (BP) was modestly, but significantly, increased at week 7, whereas (**f**) diastolic pressure and (**g**) heart rate (HR) remained unchanged (N = 5–6 per group). (**h**) Diastolic pressure in the left ventricle (LVP_{ed}) is significantly elevated at 5 and 7 weeks post-5/6Nx, suggesting diastolic dysfunction. Body weight (Wt), (**i**) normalized heart weight, and (**j**) isolated heart weight were significantly elevated as early as 2 weeks post-5/6Nx. Mass calculated (ASE) from echocardiography measurements of the LV (**k**) also indicated progressive hypertrophy. Relative wall thickness (diastolic LV wall thickness/diastolic chamber diameter) was significantly elevated at 4 and 5 weeks post-5/6Nx, indicating hypertrophic LV remodeling (*l*). N = 4–6 per group; $^{*}P < 0.05$ versus sham control at time point. $^{\#}P < 0.05$ versus indicated 5/6Nx group, 2-way analysis of variance. ASE, American Society of Echocardiography; bpm, beats per minute; Wk, week. To optimize viewing of this image, please see the online version of this article at www.kidney-international.org.

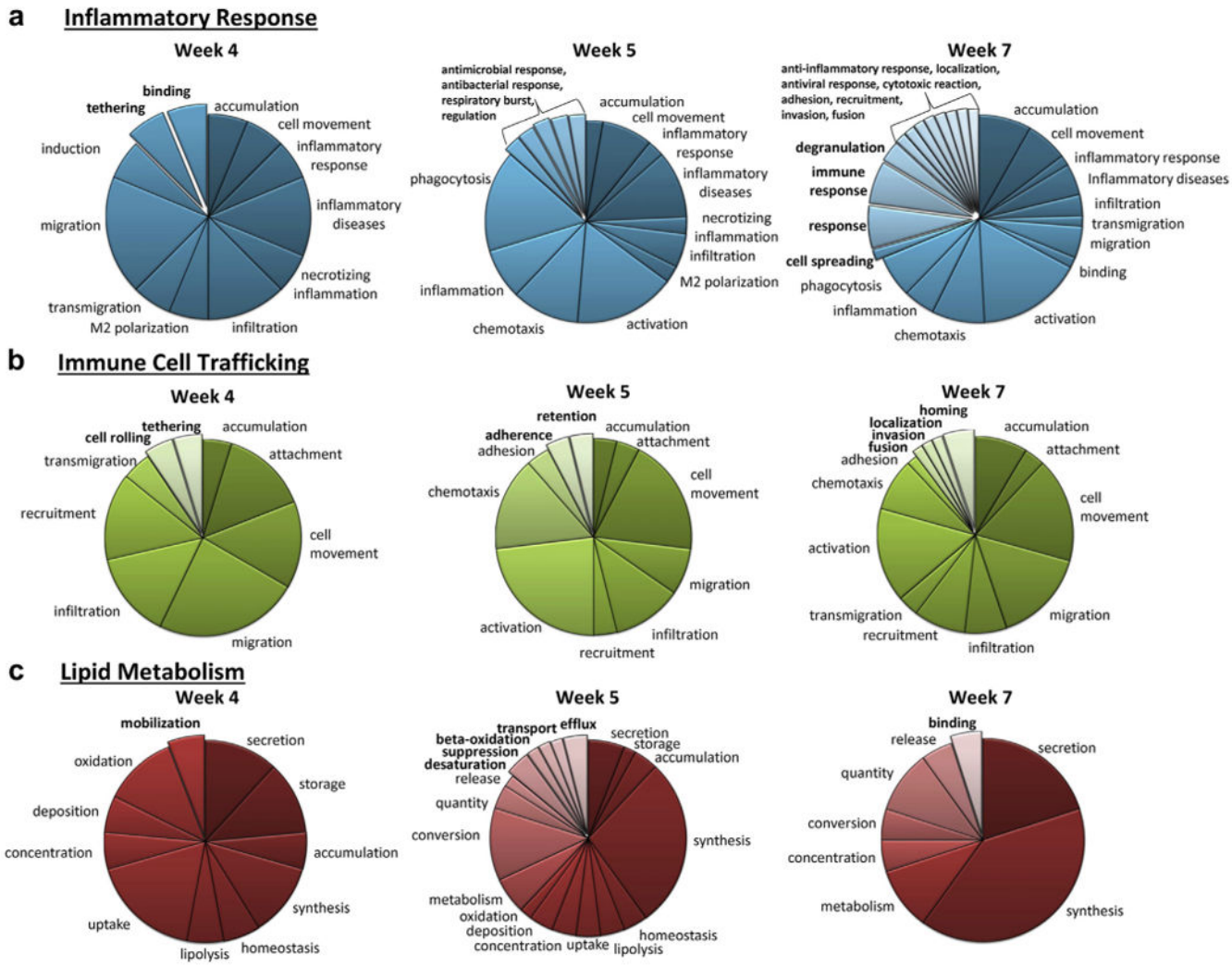

Figure 3. Ingenuity Pathway Analysis (IPA) analysis identified disease functions enriched with genes that were differentially expressed with 5/6 nephrectomy

Disease functions related to inflammatory response (a), immune cell trafficking (**b**), and lipid metabolism (c) are shown. Categories shown in bold were only identified at a single time point. See Supplementary Table S2 for a complete list of IPA-identified disease functions.

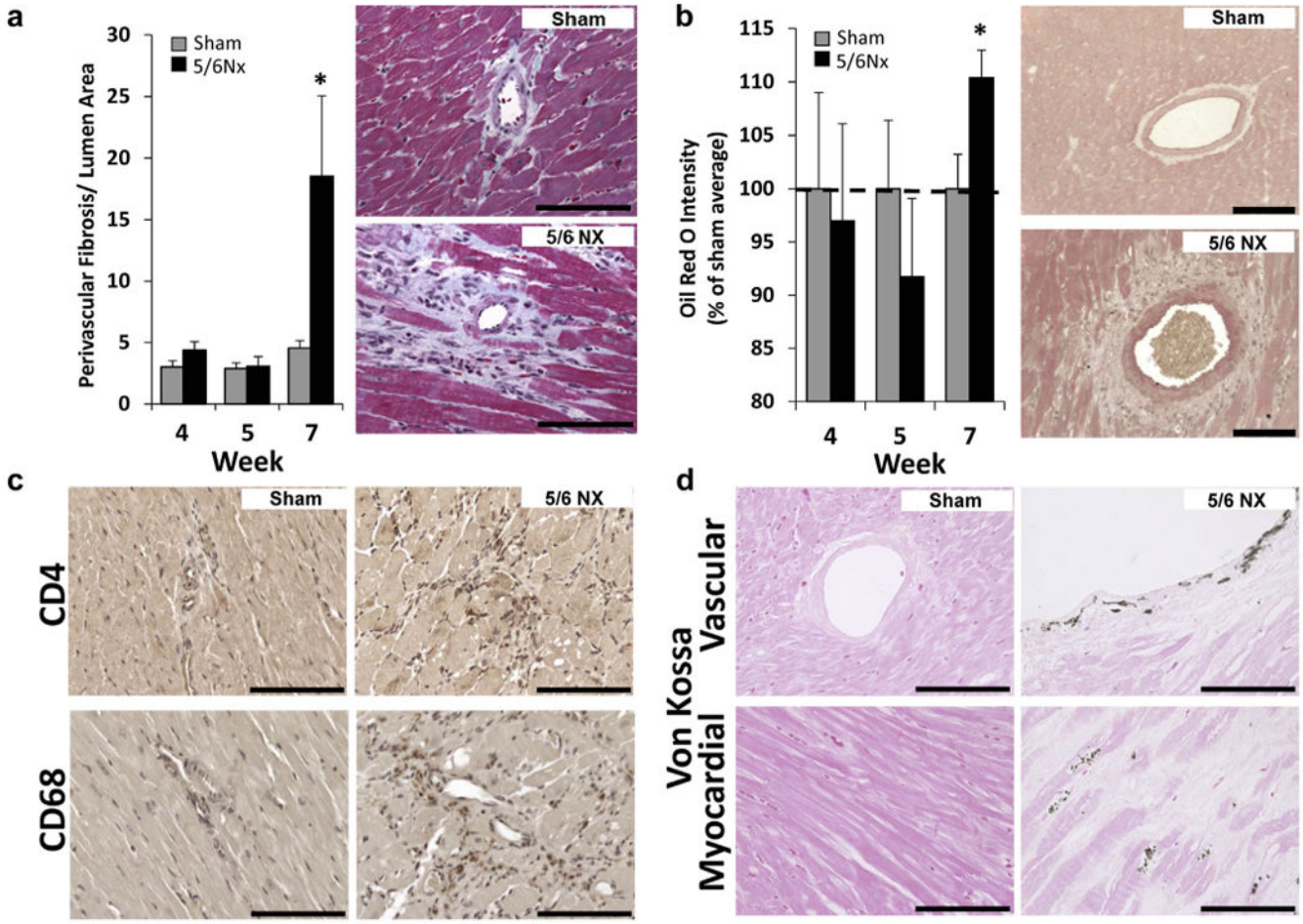

Figure 4. Left ventricular (LV) tissues exhibit limited fibrosis despite increased lipid accumulation, calcification, and immune cell infiltration 7 weeks post-5/6 nephrectomy (5/6Nx). (a) Quantification of collagenous tissue surrounding small LV arteries was significantly increased only at 7 weeks post-5/6Nx

(**b**) Similarly, LV lipid indicated by the intensity of Oil Red O stain was only increased at the 7-week time point. (c) Infiltration of immune cells (T helper and macrophages, brown stain) and (d) calcium deposition (von Kossa stain, black with eosin counterstain) were only detected in animals 7 weeks after 5/6Nx. $N = 5–6$ per group; $*P < 0.05$ versus sham controls at each time point; *t* test. Bar = 100 μm. To optimize viewing of this image, please see the online version of this article at www.kidney-international.org.

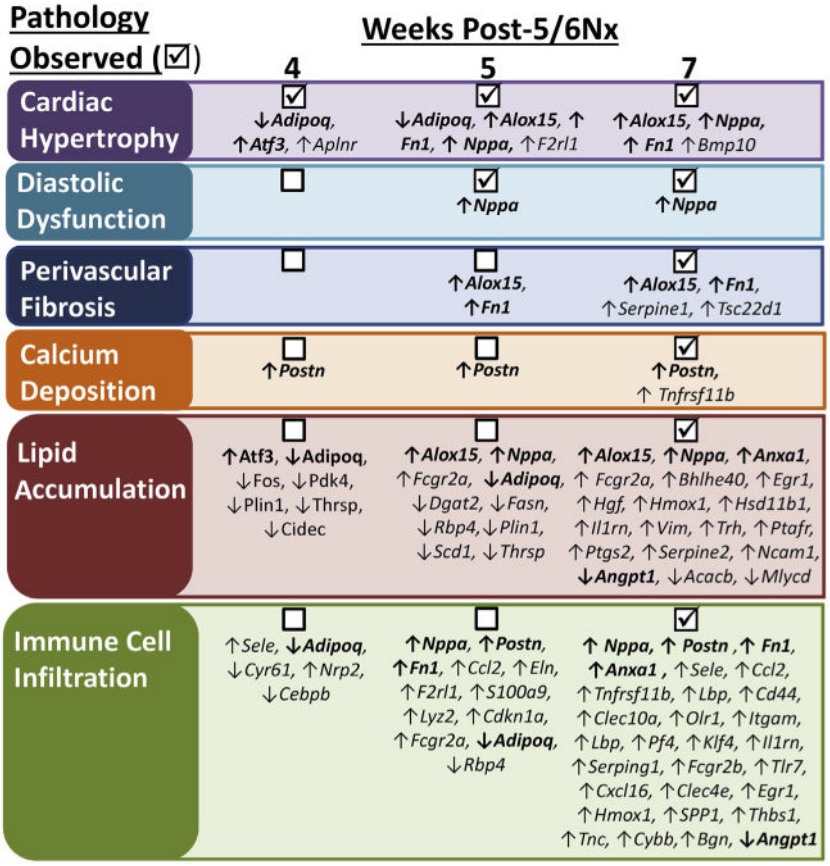

Figure 5. Summary of physiological, pathologic, and gene expression changes

IPA (Ingenuity Pathway Analysis) of differentially expressed genes at weeks 4, 5, and 7 identified disease-related functions likely to be affected. Observed pathologic changes ((x2611)) are listed with the differentially expressed genes that have been identified to be related to that process in IPA Downstream Effects Analysis. Note that in many cases, gene expression changes occur before pathology is detected. 5/6Nx, 5/6 nephrectomy.

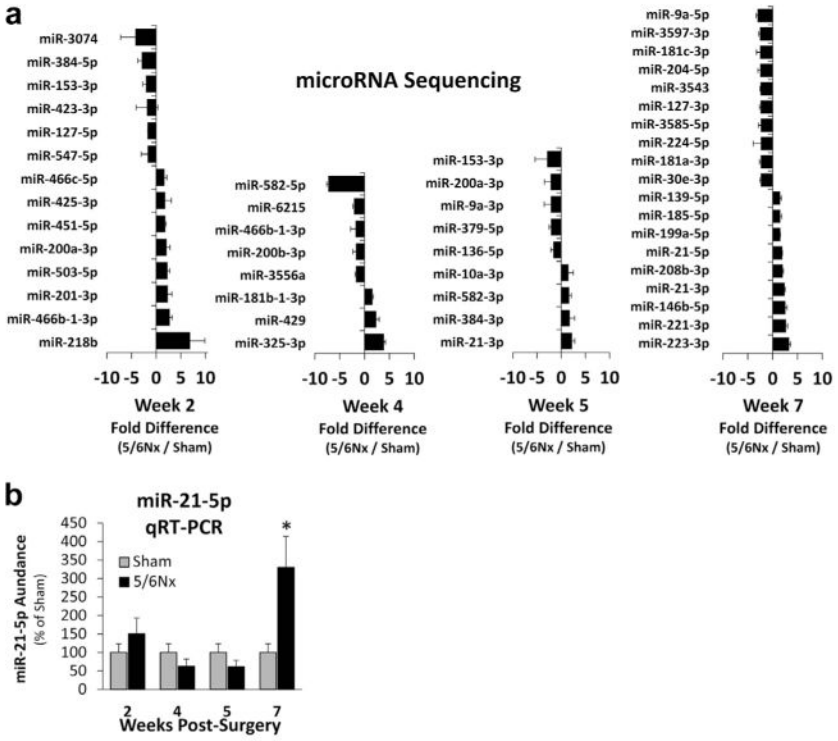

Figure 6. Left ventricular (LV) microRNA (miRNA) is temporally altered after 5/6 nephrectomy (5/6Nx) with miR-21-5p LV abundance increased at week 7 post-5/6Nx

(a) The top 10 or fewer miRNAs that were both detected in all of the pools analyzed were altered by an average of at least 1.5-fold with 5/6Nx are shown. Notably, very few of the miRNAs met these criteria at more than 1 time point, suggesting important temporal changes in miRNA abundance throughout the development of LV pathology. (b) Abundance of miR-21-5p from individual samples from the sequenced pools was analyzed by real-time quantitative reverse transcription polymerase chain reaction (qRT-PCR), confirming that LV abundance is increased at week 7 and not at earlier time points. $*P < 0.05$ versus sham at each time point, *t* test.

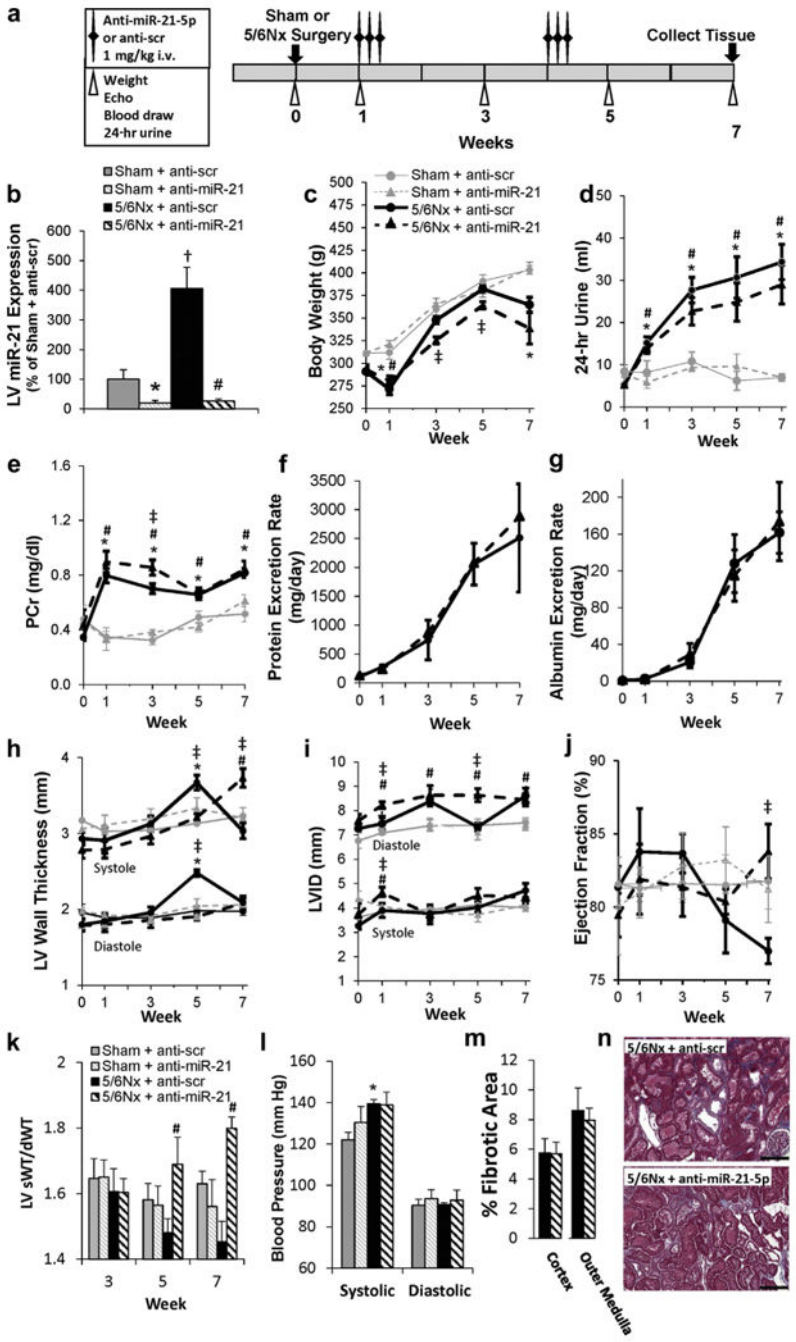

Figure 7. Suppression of miR-21-5p improves cardiac function without reducing blood pressure or kidney pathology

(a) Phenotyping protocol used. (**b**) Analysis of miR-21-5p abundance by quantitative real-time polymerase chain reaction–confirmed efficacy of anti–miR-21-5p treatment protocol until the end of the 7-week study. Repeated phenotypic measurements of body weight (c) and 24-hour urine volume (d). There was no apparent improvement in renal function in 5/6 nephrectomy (5/6Nx) rats as a result of locked nucleic acid-anti-miR-21-5p treatment, as indicated by plasma creatinine (PCr) levels (**e**), protein excretion rate (**f**), and albumin

excretion rate (**g**) (shams not analyzed). Measurements of wall thickness (**h**), left ventricular inner diameter (LVID) (i), and ejection fraction (**j**) were made by echocardiography. The systolic/diastolic wall thickness (sWT/dWT) ratio increased at weeks 5 and 7 with anti-miR-21-5p delivery (**k**), whereas blood pressure was not affected (l). Further, no reduction in renal fibrosis or morphology was observed with locked nucleic acid anti-miR-21-5p-treated animals (representative images [m], trichrome stain [**n**]). $N = 4$ to 6 per group; $^{*}P < 0.05$ anti-scrambled (scr) versus anti-miR-21-5p treatment in sham surgery; $\#P < 0.05$ anti-scr versus anti-miR-21-5p treatment in sham surgery; †5/6Nx versus sham within anti-scr treatment; $^{\ddagger}P < 0.05$ 5/6Nx versus sham in anti-miR-21-5p treatment; (a,k,l,m) 2-way analysis of variance, (**c-j**) 2-way repeated-measures analysis of variance performed in the treatment and in the surgical group at measured time points. Bar = 200 μm.To optimize viewing of this image, please see the online version of this article at www.kidney-international.org.

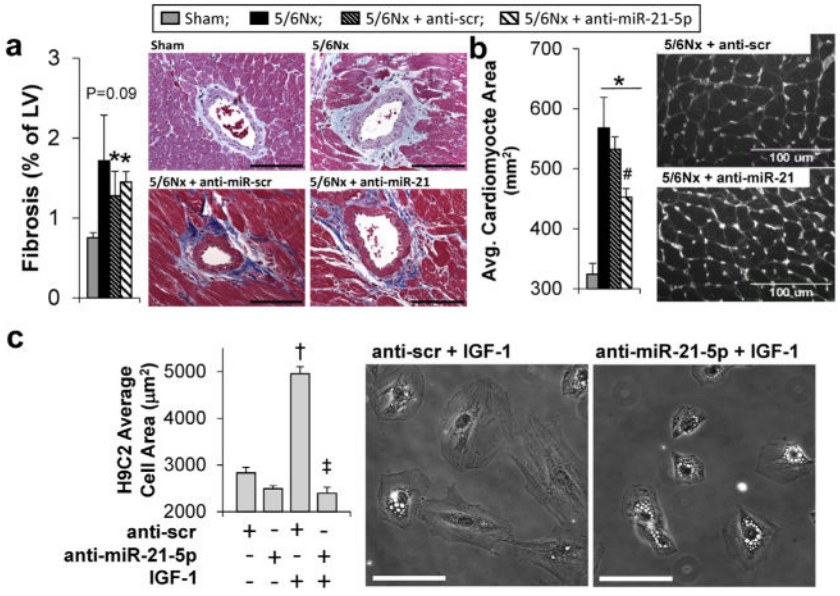

Figure 8. miR-21-5p effect on fibrosis and hypertrophy

(a) Anti-miR-21-5p treatment of 5/6 nephrectomy (5/6Nx) rats had no effect on the abundance left ventricular perivascular fibrosis; however, it significantly reduced the average cross-sectional left ventricular cardiomyocyte area in wheat germ agglutinin-treated left ventricular sections (**b**). N = 5-6 per group; $^{*}P < 0.05$ versus sham controls and $\#P < 0.05$ versus anti-scr 5/6 Nx control; 2-way analysis of variance. (c) The ability of miR-21-5p inhibition to prevent hypertrophic growth was tested in H9C2 cells treated with insulin-like growth factor (IGF-1) (50 ng/ml) for 24 hours. Transfection of cells with anti-miR-21 prevented the IGF-1 -induced increase in H9C2 area (vs. anti-scr transfected cells). N = 3 per group; $^{\dagger}P < 0.05$ versus IGF-1 control (saline), and $^{*}P < 0.05$ versus miR-21 control (anti-scr + IGF); 2-way analysis of variance. Avg., average; LV, left ventricle; scr, scrambled. Bar = 100 μm. To optimize viewing of this image, please see the online version of this article at www.kidney-international.org.

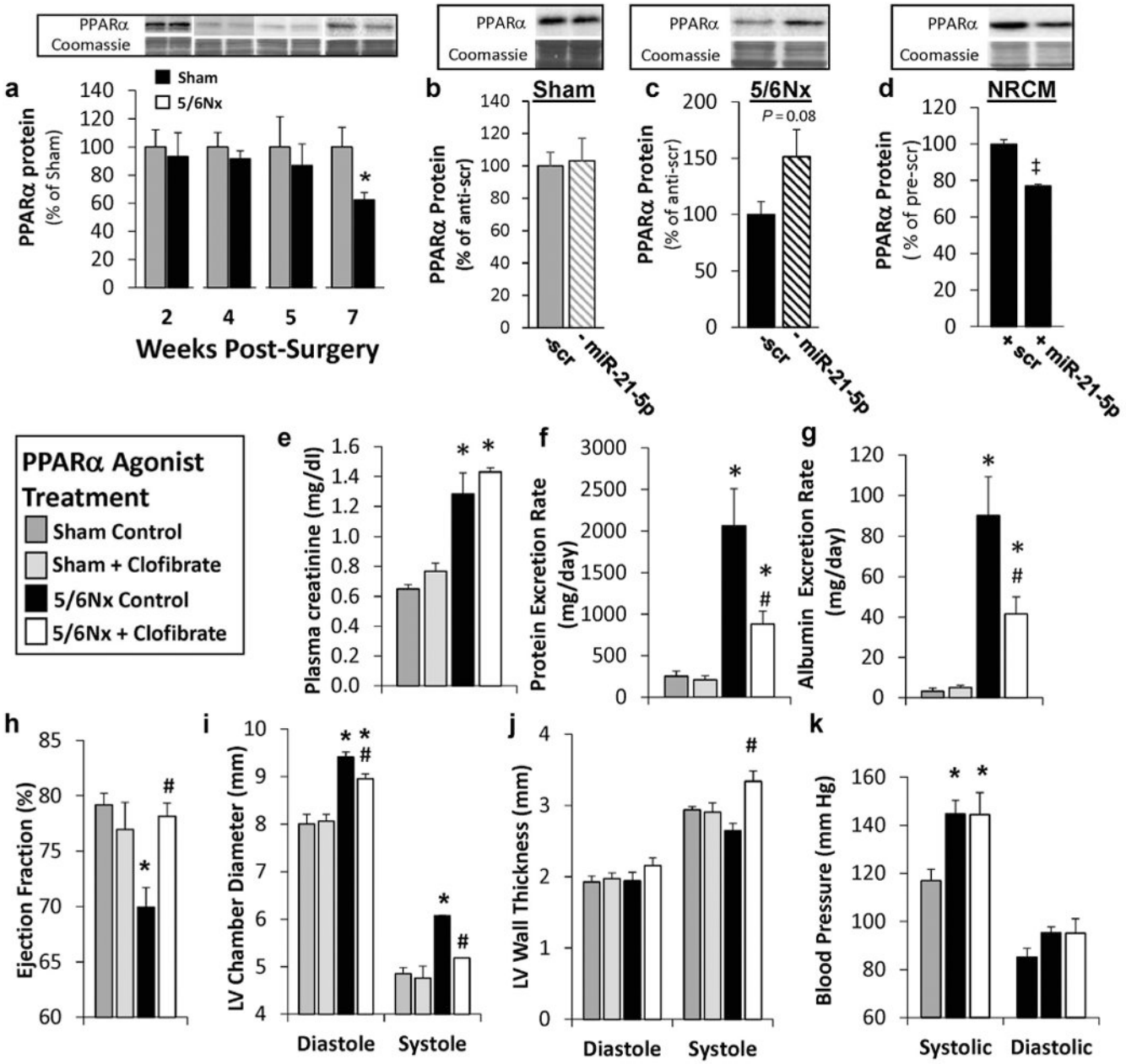

Figure 9. Peroxisome proliferator-activated receptor-α (PPARα) is regulated by miR-21-5p, and PPARα activation improves renal and cardiac function in type 4 cardiorenal syndrome

Western blot shows that (a) left ventricular (LV) PPARα is reduced with 7 weeks of 5/6 nephrectomy (5/6Nx) and (b,c) only increased with anti-miR-21-5p (— miR-21) treatment in 5/6Nx rats (*N* = 5-6). (d) Pre-miR-21-5p (+ miR-21) transfection in neonatal rat cardiomyocytes (NRCM) reduced PPARα protein abundance (*N* = 3). PPARα bands were normalized by total protein evaluated by quantification of Coomassie stain. Low-dose treatment with the PPARα agonist clofibrate improves renal cardiac function and reduces LV dilation observed 10 weeks after surgery. Daily i.p. injections of 25 mg/kg clofibrate had no effect on plasma creatinine (**e**) but reduced urinary protein (**f**) and albumin excretion (**g**) in

5/6Nx rats. Clofibrate treatment also prevented a decrease in ejection fraction (**h**) and dilation of the left ventricle (i) while increasing LV systolic wall thickness (**j**). Systolic and diastolic blood pressures were not altered by clofibrate treatment in 5/6Nx rats (**k**). Mean ± SE; $N = 4$-12 per group; $*P < 0.05$ versus sham controls in treatment; $\#P < 0.05$ versus 5/6Nx control group; ‡pre-scrambled control group to the left, $P < 0.05$, *t*-test (**a-d**), 2-way analysis of variance (**e-k**). To optimize viewing of this image, please see the online version of this article at www.kidney-international.org.

Table 1

Top 10 differentially expressed, 5/6Nx up- and down-regulated genes identified by mRNA-sequencing analysis of pooled LV tissue at 4, 5, and 7 weeks post-5/6 NX. *P* value determined by Cuffdiff analysis (see Supplemental Methods)

Upregulated									
	Week 4			Week 5			Week 7		
Rank	**Gene**	**Log ratio**	***P* value**	**Gene**	**Log ratio**	**P value**	**Gene**	**Log ratio**	***P* value**
1	*Sele*	1.374	<0.0001	*Arsi*	2.546	0.0001	*Spp1*	4.462	<0.0001
2	*Aspm*	1.213	<0.0001	*Prc1*	1.919	<0.0001	*Olr1*	3.897	<0.0001
3	*Cdk1*	1.200	<0.0001	*Cdca3*	1.875	0.0001	*Alox15*	3.853	<0.0001
4	*Fam111a*	1.130	<0.0001	*Kif23*	1.807	<0.0001	*Mt1m/Mt2A*	3.77	<0.0001
5	*Cenpf*	1.128	<0.0001	*Fam64a*	1.779	<0.0001	*Postn*	3.487	<0.0001
6	*Top2a*	1.101	<0.0001	*S100a9*	1.711	<0.0001	*Lox*	3.429	<0.0001
7	*Prc1*	1.035	<0.0001	*Cdk1*	1.687	<0.0001	*Rgs1*	3.302	<0.0001
8	*Arhgap20*	1.010	<0.0001	*Cdkn3*	1.641	<0.0001	*Trh*	3.143	<0.0001
9	*Postn*	0.907	<0.0001	*Top2a*	1.636	<0.0001	*Mt1*	3.044	<0.0001
10	*Fbn1*	0.898	<0.0001	*Ube2c*	1.626	<0.0001	*Tnfrsf11b*	2.901	<0.0001
Downregulated									
	Week 4			Week 5			Week 7		
Rank	Gene	Log ratio	*P* value	Gene	Log ratio	*P* value	Gene	Log ratio	*P* value
1	*Cidec*	-2.251	<0.0001	*Pck1*	-4.316	<0.0001	*Pdia2*	-2.939	0.00045
2	*Plin1*	-1.852	<0.0001	*Thrsp*	-4.21	<0.0001	*Gcgr*	-1.845	0.0004
3	*Adipoq*	-1.455	<0.0001	*Cidec*	-3.01	<0.0001	*Gpt*	-1.81	0.0002
4	*Thrsp*	-1.438	<0.0001	*Plin1*	-2.839	<0.0001	*Bmp10*	-1.729	<0.0001
5	*Atf3*	-1.407	<0.0001	*Atp5f1*	-2.285	<0.0001	*Scgn*	-1.651	0.0001
6	*Pck1*	-1.36	<0.0001	*Fasn*	-2.19	<0.0001	*Ucp3*	-1.614	0.0006
7	*Car3*	-1.341	<0.0001	*Scd1*	-1.9	<0.0001	*Pyroxd2*	-1.555	0.00025
8	*Abra*	-1	<0.0001	*Adipoq*	-1.812	<0.0001	*Ros1*	-1.554	<0.0001
9	*Cyr61*	-0.964	<0.0001	*Rbp4*	-1.689	<0.0001	*Tmod4*	-1.392	0.00035

Upregulated									
	Week 4			Week 5			Week 7		
Rank	Gene	Log ratio	*P* value	Gene	Log ratio	P value	Gene	Log ratio	*P* value
10	*Wfdc1*	-0.939	<0.0001	*Car3*	-1.281	<0.0001	*Ky*	-1.376	<0.0001